


Phonon-assisted insulator-metal transitions in correlated systems driven by dopingE. I. Shneyder ^{1,*}, M. V. Zotova,^{1,2} S. V. Nikolaev ^{1,2} and S. G. Ovchinnikov ^{1,2}¹*Kirensky Institute of Physics, Federal Research Center KSC SB RAS, 660036 Krasnoyarsk, Russia*²*Siberian Federal University, 660041 Krasnoyarsk, Russia* (Received 15 May 2021; revised 18 October 2021; accepted 21 October 2021; published 29 October 2021)

We consider how electron-phonon interaction influences the insulator-metal transitions driven by doping in a strongly correlated system. Using the polaronic version of the generalized tight-binding method, we investigate a multiband two-dimensional model taking into account both charge density displacement and transitive types of electron-lattice contributions. For adiabatic ratio $t \gg \omega_0$, we analyze a wide electron-phonon parameter range and demonstrate the relationship between transition features and such properties of the system as polaron and bipolaron crossovers, the redistribution of the spectral weight due to the multiparticle effects of Coulomb and electron-phonon interactions, orbital selectivity, flat-band formation, and pseudogap behavior of various origins.

DOI: [10.1103/PhysRevB.104.155153](https://doi.org/10.1103/PhysRevB.104.155153)**I. INTRODUCTION**

The mutual influence between electron-electron and electron-phonon interactions is one of the intriguing problems of condensed matter theory. It acquires particular importance in the context of the insulator-metal transition in the compounds of transition metals [1–4]. Achieving conduction switching in correlated systems with minimal energy dissipation can pave the way toward novel memory elements, low-power neuromorphic computing, or other highly energy-efficient applications [5–7]. Indeed, many oxides, sulfides, nickelates, and other systems of d metals exhibit a sharp transition from nonmetal to a metal ground state induced by relatively small alternation in temperature, pressure, strain, composition, or chemical doping [2,5,8,9]. In electronic devices, it can be driven by optical pumping [10] or applying an electrical current or voltage [11]. Despite considerable attention to the problem, the dependence of the transformation characteristics on the atomistic and electronic structures of materials remains the outstanding fundamental question. The underlying mechanisms are the subject of active discussions. These can be structural distortions, electronic instabilities, or their cooperative or competing contributions [5,12,13].

Due to significant electron correlations, a number of transition metal compounds with a half-filled band are insulators [14]. The transition from the band metal to the Mott-Hubbard insulator ground state is controlled by a ratio of the on-site Coulomb repulsion to the bandwidth [15,16]. It occurs in the same crystalline structure and can be triggered by different stimuli leading to a change in the band filling factor or the bandwidth. In many d -metal compounds, pronounced effects of strong electron-phonon interaction (EPI) indicate the insufficiency of the purely electronic picture [17–32]. The problem is extremely entangled since both Coulomb and electron-lattice interactions cause such correlation effects as

a renormalization of electron and phonon spectra, intraband and interband redistribution of the spectral weight, an increase in the effective mass, and a tendency toward localization of charge carriers.

Most studies of the mutual effects of electron-electron and electron-phonon interactions are focused on the Hubbard-Holstein model, which includes local Coulomb contribution and on-site modulation of the particle potential via lattice vibrations. Its phase diagram contains [33–37] a metallic ground state when both interactions are small, Mott-Hubbard or charge-density wave insulating states, driven by Coulomb or electron-phonon interactions, respectively, and a variety [38–41] of phases caused by competing orders. Here, we essentially consider an extension of this model, accounting for the multiband effects and off-site electron-phonon coupling, which modulates [42–44] the kinetic energy of charge carriers. It has been shown earlier that multiorbital contributions significantly modify the phase diagram of the Hubbard-Holstein model [45] at half filling. For small Coulomb coupling and intermediate or strong electron-lattice ones, the presence of nonequivalent bands leads to the occurrence of an orbital-selective insulating Peierl’s phase, which precedes the transition to the insulating state of charge density waves. In this phase, we can expect a non-Fermi-liquid behavior of charge carriers, similar to that observed [46,47] in the orbital-selective Mott phase [48,49] for the Ising Hund’s coupling.

The nontrivial behavior of the system can also result from the Barišić-Labbé-Friedel-Su-Schrieffer-Heeger type contribution of the electron-phonon interaction. The modulation of orbital overlaps is characterized by the coupling parameter depending on both boson momentum and the particle one and being off-diagonal in a real-space representation. Such formulation of the problem goes beyond the applicability of the Gerlach-Löwen theorem, which rules out the nonanalyticities in the ground state properties of the polaron system if coupling strength is constant or depends on boson momentum only [50]. The revision of the concept of smoothly varying polaron properties starts from the demonstrations of the nonanalyticity

*eshneyder@gmail.com

in the entanglement entropy [51] and the sharp transition in the ground state energy [52] of the polaron system. Another critical consequence of the transitive contribution is the formation of light bipolarons, which are stable against large values of the screened Coulomb repulsion [52,53].

In this paper, we are interested in the general features of the insulator-metal transitions driven by doping in the particle-phonon coupled systems. We restrict our attention to the limit of strong electron correlations and assume the phonon field energy inherent for most compounds, $\omega_0 \ll t$. Our systematic analysis is based on the two-dimensional three-orbital pd model, which is relevant primarily for layered copper oxides. Nevertheless, it illustrates some evolution lows of transition behavior in correlated materials. Previously, we discussed the Peierl's type of metal-insulator transitions controlled by electron-phonon interaction in the underdoped compound [54]. Here we show how the electron-phonon interaction can affect the Mott-Hubbard transitions via flat-band formation and hybridizing fermionic bands with Frank-Condon resonances. It turns out that crossovers of polaron and bipolaron properties can predict characteristics of transitions that differ in the rate and amplitude of changes in the density of states of charge carriers.

II. MODEL AND METHOD

The total Hamiltonian reads $H = H^{el} + H^{ph} + H^{epi}$, where

$$\begin{aligned}
 H^{el} = & \sum_{\mathbf{g},\sigma} (\varepsilon_d - \mu) n_{\mathbf{g},\sigma}^d + \sum_{\mathbf{g}} U_d n_{\mathbf{g},\sigma}^d n_{\mathbf{g},-\sigma}^d \\
 & + \sum_{\mathbf{g},\mathbf{r},\sigma} (\varepsilon_p - \mu) n_{\mathbf{g}+\mathbf{r},\sigma}^p + \sum_{\mathbf{g},\mathbf{r}} U_p n_{\mathbf{g}+\mathbf{r},\sigma}^p n_{\mathbf{g}+\mathbf{r},-\sigma}^p \\
 & + \sum_{(\mathbf{g},\mathbf{g}'),\mathbf{r},\mathbf{r}',\sigma} P_{\mathbf{r}\mathbf{r}'} t_{pp} (p_{\mathbf{g}+\mathbf{r},\sigma}^\dagger p_{\mathbf{g}'+\mathbf{r}',\sigma} + \text{H.c.}) \\
 & + \sum_{\mathbf{g},\mathbf{r},\sigma} P_{\mathbf{r}} t_{pd} (d_{\mathbf{g},\sigma}^\dagger p_{\mathbf{g}+\mathbf{r},\sigma} + \text{H.c.}) \\
 & + \sum_{\mathbf{g},\mathbf{r},\sigma,\sigma'} V_{pd} n_{\mathbf{g}+\mathbf{r},\sigma}^p n_{\mathbf{g},\sigma'}^d, \quad (1)
 \end{aligned}$$

$$H^{ph} = \sum_{\mathbf{g}} \hbar\omega_0 \left(f_{\mathbf{g}}^\dagger f_{\mathbf{g}} + \frac{1}{2} \right), \quad (2)$$

$$\begin{aligned}
 H^{epi} = & \sum_{\mathbf{g},\sigma} M_d (f_{\mathbf{g}}^\dagger + f_{\mathbf{g}}) d_{\mathbf{g}\sigma}^\dagger d_{\mathbf{g}\sigma} \\
 & + \sum_{\mathbf{g},\mathbf{r},\sigma} M_{pd} P_{\mathbf{r}} (f_{\mathbf{g}}^\dagger + f_{\mathbf{g}}) (d_{\mathbf{g}\sigma}^\dagger p_{\mathbf{g}+\mathbf{r},\sigma} + \text{H.c.}). \quad (3)
 \end{aligned}$$

The Hamiltonian (1) describes the low-energy physics of the CuO plane, which is a common structural unit in complex copper oxides with a partially filled $3d$ orbital. Operators $d_{\mathbf{g},\sigma}^\dagger$ and $p_{\mathbf{g}+\mathbf{r},\sigma}^\dagger$ create a hole with spin σ on $d_{x^2-y^2}$ -copper and $p_{x(y)}$ -oxygen atomic orbitals at positions indicated by vectors \mathbf{g} or $\mathbf{g} + \mathbf{r}$, respectively. Vector \mathbf{r} goes over oxygen atom positions in the square unit cell at site \mathbf{g} . The values ε_d and ε_p are the local energies of the corresponding atomic orbitals, $n_{\mathbf{g},\sigma}^d$ and $n_{\mathbf{g}+\mathbf{r},\sigma}^p$ are the hole number operators, t_{pp} and t_{pd} are the hopping parameters, U_p , U_d , and V_{pd} are Coulomb repulsion

parameters, μ is the chemical potential, and $P_{\mathbf{r}}$ and $P_{\mathbf{r}'}$ are the phase factors. Depending on whether orbitals with real wave functions have the same or opposite sign in the overlap region, the phase factors are equal to 1 or -1 .

In the free phonon term (2), we consider the bond-stretching optical vibrations with energy ω_0 . The Hamiltonian H^{epi} defines charge carriers that are linearly coupled to this dispersionless mode through the modulation of the copper on-site energy and the copper-oxygen hopping energy. These electron-phonon interactions are characterized by M_d and M_{pd} parameters of the on-site or charge density displacement and the off-site or transitive contributions, respectively.

Throughout the paper we use the following set of parameters: $\varepsilon_d = 0$, $\varepsilon_p = 1.5$, $t_{pp} = 0.86$, $t_{pd} = 1.36$, $U_d = 9$, $U_p = 4$, $V_{pd} = 1.5$, $W = 2.15$, and $\omega_0 = 0.090$ (all in eV). Below, the dimensionless electron-phonon coupling constants are defined as $\lambda_{\text{on(off)}} = M_{d(pd)}^2 / W \hbar \omega_0$, where W is the bandwidth.

To study the problem, we employ the polaronic version of the generalized tight-binding (pGTB) method. A detailed description of this type of cluster perturbation theory is provided elsewhere [54–56]. In contrast to the Lanczos method, we exactly determine all eigenstates of the CuO₄ cluster Hamiltonian and then discard the highest excited states in a controlled manner, preserving the character of the spectrum. Truncating the Hilbert space of phonons, we control the convergence of the ground and the first excited states energies with 0, 1, or 2 holes per site with an error of no more than 1%. Optimization of the local basis allows us to efficiently compute the band structure of the correlated system from weak to strong electron-phonon coupling. Here, we simulate the intercluster contribution in the generalized mean-field approximation, taking into account the interaction of charge carriers with spin fluctuations. Each time we change the concentration of doped holes x or the parameters of the electron-phonon interaction λ_{on} and λ_{off} , the band structure and the chemical potential of the system are recomputed. We do not consider the effect of temperature here, leaving this problem for future research.

III. RESULTS

All results are collected below on the phase diagram in the plane of the on-site and off-site EPI parameters. To identify the patterns in the transition behavior, we compare them with polaron $\langle n_1^d \rangle_0$ and bipolaron $\langle n_2^d \rangle_0$ properties, characterizing the average number of charge carriers on the d orbitals of copper in the single- and two-particle ground states of the unit cell cluster, respectively (see Fig. 1). The total hole occupation of the copper orbitals increases with increasing on-site electron-lattice interaction. It is accompanied by continuous or discontinuous crossovers of the $\langle n_1^d \rangle_0$ and $\langle n_2^d \rangle_0$ functions with respect to the λ_{on} parameter. We find that red and blue crossover curves in Fig. 2 uniquely correlate with the type of the band structure transformation upon doping and, thus, determine the transition regimes.

A. Phase diagram

First of all, we consider the system, neglecting the electron-phonon interaction. At half filling, narrow subbands of

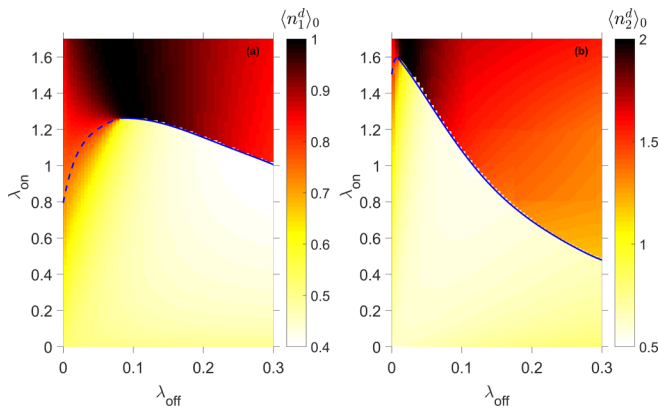


FIG. 1. Local (a) polaron $\langle n_1^d \rangle_0$ and (b) bipolaron $\langle n_2^d \rangle_0$ properties, characterizing the average number of charge carriers on the d orbitals of copper in the single- and two-particle ground states of the unit cell cluster, respectively. Here, λ_{on} is on-site parameter of electron-phonon contribution and λ_{off} is off-site one. Solid curves indicate the boundary of abrupt and discontinuous increases of the $\langle n_1^d \rangle_0$ or $\langle n_2^d \rangle_0$ values. The corresponding dashed curves mark the inflection points of these values as a function of λ_{on} parameter.

correlated d electrons and a wide band of valence p electrons of oxygen form the band structure of a charge-transfer insulator. The pd hybridization leads to the mixing of the orbitals and the broadening of the correlated bands. Upon hole doping, we reveal the chemical potential in the gap near the bottom of the conduction band. It is located here up to some critical value of $x = x_{c0}$, where $x_{c0} \approx 0.8\%$. For undoped systems,

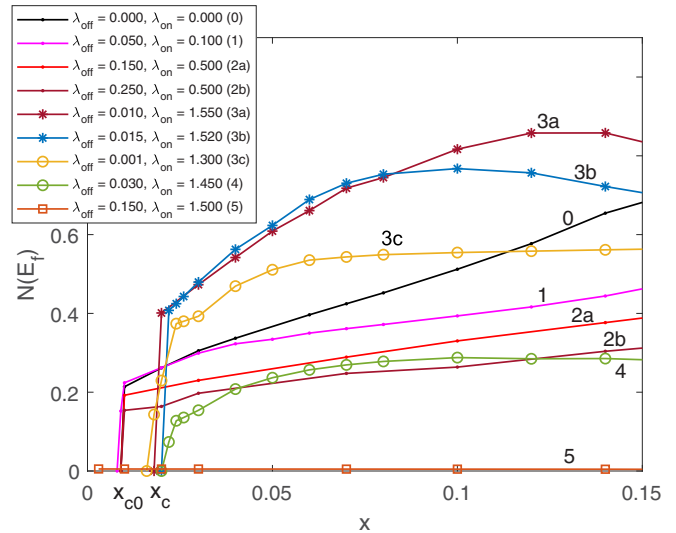


FIG. 3. Doping dependence of the density of states at the Fermi level. Zero (curve 0) or weak (curve 1) electron-phonon interaction results in the sharp transitions at $x = x_{c0}$. Intermediate interaction with dominating off-site contribution keeps the type of transition but reduces the final density of states $N(E_f)$ (curves 2a and 2b). The largest amplitude of changes in the density of states and sharp transition at $x_c > x_{c0}$ is observed with the prevailing on-site contribution (curves 3a and 3b). This transition is fast but smooth if $\lambda_{\text{off}} = 0$ (curve 3c). The formation of the flat band near the Fermi level can change the type of the transition and reduce its amplitude (curve 4). Strong electron-phonon interaction localizes the charge carriers (curve 5).

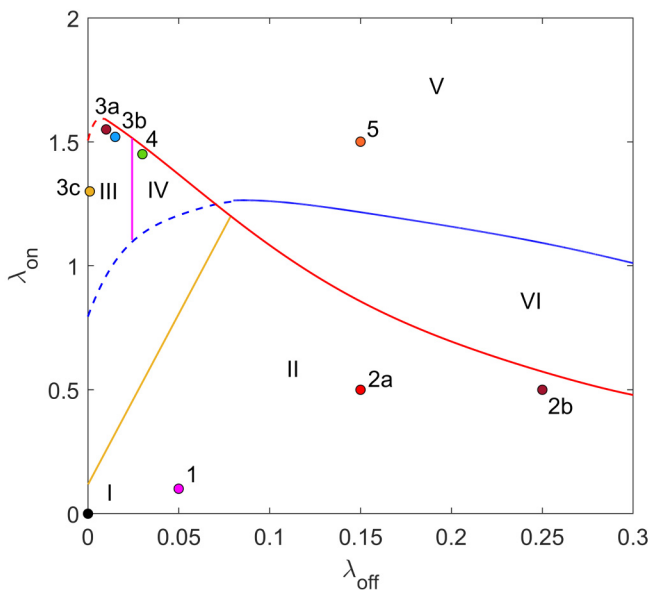


FIG. 2. Phase diagram of the system in the plane of on-site and off-site electron-phonon interaction parameters. The blue and red curves trace the crossovers in the properties of the polaron $\langle n_1^d \rangle_0$ and bipolaron $\langle n_2^d \rangle_0$ functions, respectively. Solid (dashed) lines correspond to singular (continuous) crossovers. To the left (right) of the yellow curve, the on-site (off-site) contribution prevails. The Roman numerals indicate the parameter regions with different types of the band structure transformations. The point numbers correspond to the numbers of the curves in Fig. 3.

such behavior reflects the absence of electron-hole symmetry. The latter guarantees the chemical potential is in the middle of the energy gap for a band insulator or a half-filled one-band Hubbard model [57,58]. The chemical potential confinement effect appears to be the result of the interband redistribution of the spectral weight caused by the Coulomb correlations. At sufficiently large value of the Coulomb interaction $U \geq 20$ eV or zero hybridization $t_{pd} = 0$, we find the chemical potential near the top of the valence band. Then the insulator-metal transition occurs for any nonzero value of the doped carriers, which is consistent with the paper [59]. Anyway, the chemical potential gradually enters into the band upon doping, opening the Fermi surface with a maximum of the spectral weight at the $(\pi/2, \pi/2)$ point of the Brillouin zone. As a result, we observe a sharp transition from an antiferromagnetic Mott insulator to a metallic ground state, which is characterized by an abrupt increase in the density of states of charge carriers at the Fermi level $N(E_f)$ (Fig. 3, curve 0). Weak electron-phonon interaction does not qualitatively affect the spectrum and behavior of the system (Fig. 3, curve 1; Fig. 2, part I). Slight smearing of the bands by the Frank-Condon resonances insignificantly decreases the spectral weight and density of states of quasiparticles emerging on the Fermi surface.

In contrast, strong electron-phonon interaction (Fig. 2, part V), leading to the Peierl's type of transition from itinerant to localized carriers at any fixed doping level, causes a rigid behavior of polaron system upon doping. In this regime, we do not observe a transition with an increase in the concentration of hole-doped carriers up to $x = 25\% - 30\%$

(Fig. 3, curve 5). A similar conclusion was previously obtained for the Hubbard-Holstein model using determinant Monte Carlo simulation [34]. In the phase diagram, the strong interaction part is located above both polaron and bipolaron crossover curves, where functions $\langle n^d \rangle_0$ and $\langle n^p \rangle_0$ reach their maximum values. So the distribution of the charge carrier density in the lattice among copper and oxygen orbitals takes the form of a checkerboard. Part VI of the phase diagram is characterized by moderately strong EPI effects. Between curves of singular polaron and bipolaron crossovers, the system demonstrates transition to the state with a low density of electron carriers.

Intermediate electron-lattice coupling determines the doping transformations of the system between these two limits. To the right of the yellow line (Fig. 2, part II), the off-site EPI contribution dominates. It is accompanied by a gradual increase of the band structure incoherence. As a result, we observe the transition to states with a significantly lower value of $N(E_f)$ density of charge carriers (Fig. 3, curves 2a and 2b).

To the left of the yellow line and between the crossover curves (Fig. 2, parts III and IV), the dominant on-site contribution of EPI causes qualitative changes in the band structure formation, which depend on the following circumstances. (i) The electron-phonon interaction tends to localize the charge carriers on the d orbitals of copper, so the pd hybridization weakens, and the spectral weight of the quasiparticle excitations is redistributed. At half filling, the chemical potential gets stuck at Franck-Condon in-gap states with a low spectral weight near the bottom of the conduction band. Now the electron-phonon interaction restrains the transition up to some critical value of the doped carriers $x_c > x_{c0}$, where $x_c \approx 2\% - 3\%$ (Fig. 3, curves 3 and 4). (ii) Simultaneously, a narrow flat band with a doping-dependent spectral weight begins to form around the (π, π) point of the Brillouin zone [54]. For this parameter range, low-energy polaronic excited states are bound, so the phonon spectral function demonstrates the emergence of the novel states below the one-phonon continuum [54]. Transitions between bound polaronic excited states and bipolaronic ground states cause the flat-band formation. This band is located just below the top of the valence band, but with an increase in the strength of the off-site electron-phonon coupling, its position gradually becomes higher. If the chemical potential passes through the gap under doping and first enters the valence band at the $(\pi/2, \pi/2)$ point, then a sharp insulator-metal transition occurs (curves 3a and 3b). Note that according to the Gerlach-Löwen theorem, such transition is smooth, albeit very fast, for a purely local EPI contribution (curve 3c). Due to the multiparticle effects of the spectral weight redistribution, the amplitude of the changes in the density of states $N(E_f)$ now significantly exceeds that observed at low or zero EPI (Fig. 3, curves 3a, 3b, and 3c versus curves 0–2). Otherwise, the chemical potential first falls into the flat band of impurity polaron states. This leads to a smooth transition with a smaller amplitude and slow increase in the density of states $N(E_f)$ upon doping (Fig. 3, curve 4).

B. Discussion

It turns out the crossover regime (Fig. 2, parts III and IV) correlates with the mode of the orbital-selective insulator-

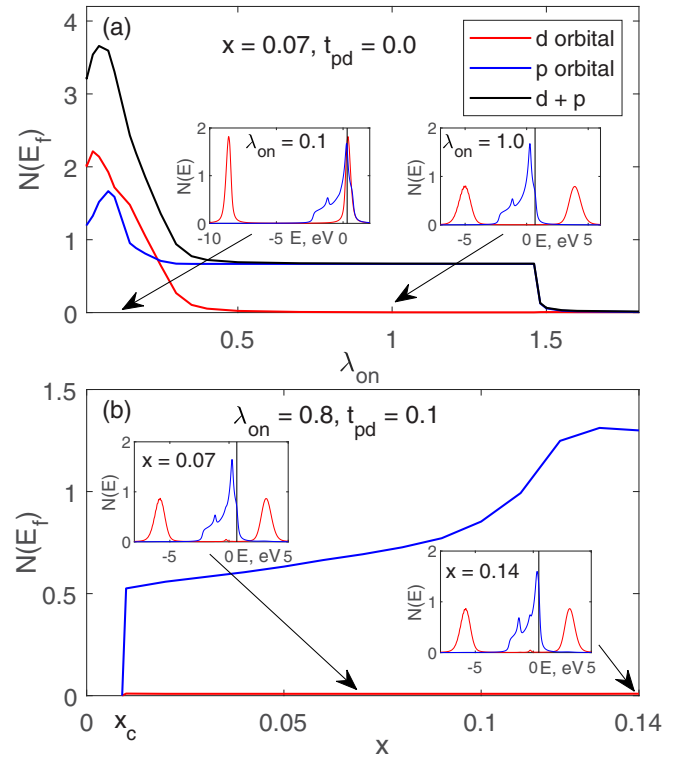


FIG. 4. Orbital-selective insulator-metal transition driven by (a) on-site electron-phonon interaction or (b) doping. The insets show the partial density of states.

metal transition observed at fixed doping level when any interorbital contributions are neglected [Fig. 4(a), $t_{pd} = 0$, $V_{pd} = 0$, $\lambda_{off} = 0$]. Similarly to the orbital-selective Mott transition [48], electron-phonon interaction first localizes the charge carriers in the narrow d orbital at $\lambda_{on} \geq 0.5$, while the wide p band remains itinerant up to strong EPI, characterized by $\lambda_{on} = 1.5$. Any hybridization effects tend to suppress the orbital-selective phase. With a fairly small contribution of the interorbital overlapping t_{pd} we observe the orbital-selective insulator-metal transition driven by doping [Fig. 4(b), initial parameters of the band structure but $t_{pd} = 0.1$ eV], but there is no orbital-selective transition upon doping for the initial parameter set. Nevertheless, the orbital-selective correlations persist and strongly influence the spectral weight redistribution between copper and oxygen orbitals at the dominating on-site electron-phonon contribution, especially in the crossover regime III and IV of the phase diagram.

Moreover, we find that the intermediate lattice contribution, which causes transitions in the crossover regime (Fig. 2, parts III and IV) at doping level $x = x_c$, leads to the pronounced pseudogap Fermi surface formation for $x \gg x_c$. Indeed, for the weak or zero electron-phonon interaction, spectral weight mapping in k space at the Fermi level demonstrates small hole pockets centered around the $(\pi/2, \pi/2)$ point of the Brillouin zone [Fig. 5(a)]. It corresponds to the short-range antiferromagnetic spin liquid state of the system. However, for parts III and IV of the phase diagram (Fig. 2), we observe [54] short or elongated Fermi arcs centered around

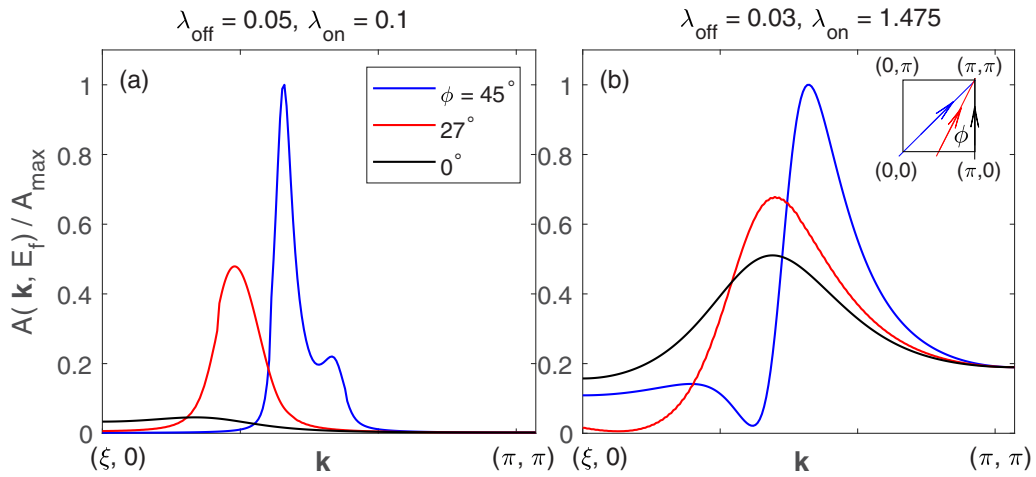


FIG. 5. Spectral weight mapping at the Fermi level as a function of the direction in the Brillouin zone for (a) weak and (b) intermediate EPI (parts I and III of the phase diagram, respectively). (b) Fermi arc is elongated and has no “backside of the pocket” if it results from the flat band formation. Parameters correspond to point 4 in Fig. 2 and curve 4 in the Fig. 3.

the point (π, π) and having a maximum spectral weight at their centers [Fig. 5(b)]. The origin of the arcs can differ and results from either the appearance of the flat band at the Fermi level (elongated arcs) or the spectral weight redistribution between the inner and outer sides of the pockets (short arcs). The later effect is inherent for systems with strong electron correlations and is significantly enhanced here due to the orbital-selective correlations and flat-band formation caused by electron-phonon interaction.

IV. CONCLUSIONS

Finally, we reveal different types of insulator-metal transitions driven by doping in the system with competing Coulomb and electron-phonon interactions. In the limit of strong electron correlations and for the parameter range between the crossovers of the polaron and bipolaron properties, the intermediate electron-lattice coupling with dominating on-site contribution causes related effects such as orbital-selective behavior, pseudogap formation, the emergence of the novel states below the one-phonon continuum in the phonon spectral function, and sharp insulator-metal transitions with the largest amplitude of the changes of the charge carrier density states at the Fermi level.

We show that the occupancy of orbitals, triggering the insulator-metal transition and relating to its features, essentially depends on both the Coulomb and electron-phonon interactions. The presented results can direct the search for new promising materials with exceptional characteristics of the insulator-metal transitions. Previously, the control of conductivity by manipulating the filling of the orbitals has been demonstrated in thin films of vanadium dioxide [60]. Note that the suppression of the electron-phonon interaction due to the effects of the Fermi blockade [61] or screening [62,63] does not change our general conclusions. In high-temperature superconductors, these phenomena develop upon doping, while transitions discussed here occur at electron concentrations close to half filling.

ACKNOWLEDGMENTS

The reported study was funded by the Russian Foundation for Basic Research, Government of Krasnoyarsk Territory, and Krasnoyarsk Regional Fund of Science according to the research project “Studies of superexchange and electron-phonon interactions in correlated systems as a basis for searching for promising functional materials,” No. 20-42-240016.

-
- [1] G. G. Guzmán-Verri, R. T. Brierley, and P. B. Littlewood, *Nature (London)* **576**, 429 (2019).
 - [2] M. Husanu, L. Vistoli, C. Verdi, A. Sander, V. Garcia, J. Rault, F. Bisti, L. L. Lev, T. Schmitt *et al.*, *Commun. Phys.* **3**, 62 (2020).
 - [3] E. Baldini, M. A. Sentef, S. Acharya, T. Brumme, E. Sheveleva, F. Lyzwa, E. Pomjakushina, C. Bernhard, M. van Schilfgaarde, F. Carbone *et al.*, *Proc. Natl. Acad. Sci. USA* **117**, 6409 (2020).
 - [4] A. Parija, J. V. Handy, J. L. Andrews, J. Wu, L. Wangoh, S. Singh, C. Jozwiak, A. Bostwick, E. Rotenberg, W. Yang *et al.*, *Matter* **2**, 1166 (2020).
 - [5] J. L. Andrews, D. A. Santos, M. Meyyappan, R. S. Williams, and S. Banerjee, *Trends Chem.* **1**, 711 (2019).
 - [6] Y. Kalcheim, A. Camjayi, J. del Valle, P. Salev, M. Rozenberg, and I. K. Schuller, *Nat. Commun.* **11**, 2985 (2020).
 - [7] N. Shukla, A. Thathachary, A. Agrawal, H. Paik, A. Aziz, D. G. Schlom, S. K. Gupta, R. Engel-Herbert, and S. Datta, *Nat. Commun.* **6**, 7812 (2015).
 - [8] D. Adler, *Rev. Mod. Phys.* **40**, 714 (1968).
 - [9] M. Imada, A. Fujimori, and Y. Tokura, *Rev. Mod. Phys.* **70**, 1039 (1998).
 - [10] J. Lourembam, A. Srivastava, C. La-o-vorakiat, L. Cheng, T. Venkatesan, and E. E. M. Chia, *Sci. Rep.* **6**, 25538 (2016).

- [11] A. Asamitsu, Y. Tomioka, H. Kuwahara, and Y. Tokura, *Nature (London)* **388**, 50 (1997).
- [12] F. Grandi, A. Amaricci, and M. Fabrizio, *Phys. Rev. Research* **2**, 013298 (2020).
- [13] Y. Ji, L. Cheng, N. Li, Y. Yuan, W. Liang, and H. Yang, *J. Phys.: Condens. Matter* **33**, 105603 (2020).
- [14] N. F. Mott, *Rev. Mod. Phys.* **40**, 677 (1968).
- [15] J. Hubbard, *Proc. R. Soc. London A* **276**, 238 (1963).
- [16] J. Hubbard, *Proc. R. Soc. London A* **281**, 401 (1964).
- [17] L. Pintschovius, *Phys. Status Solidi (b)* **242**, 30 (2005).
- [18] D. Reznik, L. Pintschovius, J. M. Tranquada, M. Arai, Y. Endoh, T. Masui, and S. Tajima, *Phys. Rev. B* **78**, 094507 (2008).
- [19] A. Bianconi, N. L. Saini, A. Lanzara, M. Missori, T. Rossetti, H. Oyanagi, H. Yamaguchi, K. Oka, and T. Ito, *Phys. Rev. Lett.* **76**, 3412 (1996).
- [20] S. H. Pan, J. P. O'Neal, R. L. Badzey, C. Chamon, H. Ding, J. R. Engelbrecht, Z. Wang, H. Eisaki, S. Uchida, A. K. Gupta *et al.*, *Nature (London)* **413**, 282 (2001).
- [21] Z. Islam, X. Liu, S.K. Sinha, J. C. Lang, S.C. Moss, D. Haskel, G. Srajer, P. Wochner, D.R. Lee, D.R. Haefner, and U. Welp, *Phys. Rev. Lett.* **93**, 157008 (2004).
- [22] G. Meng Zhao, H. Keller, and K. Conder, *J. Phys.: Condens. Matter* **13**, R569 (2001).
- [23] D. Rubio Temprano, K. Conder, A. Furrer, H. Mutka, V. Trounov, and K. A. Müller, *Phys. Rev. B* **66**, 184506 (2002).
- [24] D. Rubio Temprano, J. Mesot, S. Janssen, A. Furrer, K. Conder, and H. Mutka, *Phys. Rev. Lett.* **84**, 1990 (2000).
- [25] M. Bendele, F. von Rohr, Z. Guguchia, E. Pomjakushina, K. Conder, A. Bianconi, A. Simon, A. Bussmann-Holder, and H. Keller, *Phys. Rev. B* **95**, 014514 (2017).
- [26] D. Mihailović, C. M. Foster, K. Voss, and A. J. Heeger, *Phys. Rev. B* **42**, 7989 (1990).
- [27] X.-X. Bi and P. C. Eklund, *Phys. Rev. Lett.* **70**, 2625 (1993).
- [28] G. Zhao, M. B. Hunt, H. Keller, and K. A. Müller, *Nature (London)* **385**, 236 (1997).
- [29] A. Damascelli, Z. Hussain, and Z.-X. Shen, *Rev. Mod. Phys.* **75**, 473 (2003).
- [30] K. M. Shen, F. Ronning, W. Meevasana, D. H. Lu, N. J. C. Ingle, F. Baumberger, W. S. Lee, L. L. Miller, Y. Kohsaka, M. Azuma, M. Takano, H. Takagi, and Z. X. Shen, *Phys. Rev. B* **75**, 075115 (2007).
- [31] N. P. Armitage, F. Ronning, D. H. Lu, C. Kim, A. Damascelli, K. M. Shen, D. L. Feng, H. Eisaki, Z.-X. Shen, P. K. Mang *et al.*, *Phys. Rev. Lett.* **88**, 257001 (2002).
- [32] R. Khasanov, A. Shengelaya, D. Di Castro, E. Morenzoni, A. Maisuradze, I. M. Savić, K. Conder, E. Pomjakushina, A. Bussmann-Holder, and H. Keller, *Phys. Rev. Lett.* **101**, 077001 (2008).
- [33] G. S. Jeon, T.-H. Park, J. H. Han, H. C. Lee, and H.-Y. Choi, *Phys. Rev. B* **70**, 125114 (2004).
- [34] C. B. Mendl, E. A. Nowadnick, E. W. Huang, S. Johnston, B. Moritz, and T. P. Devereaux, *Phys. Rev. B* **96**, 205141 (2017).
- [35] S. Sayyad, R. Žitko, H. U. R. Strand, P. Werner, and D. Golež, *Phys. Rev. B* **99**, 045118 (2019).
- [36] P. Werner and A. J. Millis, *Phys. Rev. Lett.* **99**, 146404 (2007).
- [37] Z. Han, S. A. Kivelson, and H. Yao, *Phys. Rev. Lett.* **125**, 167001 (2020).
- [38] S. Kumar and J. van den Brink, *Phys. Rev. B* **78**, 155123 (2008).
- [39] J. Bauer and A. C. Hewson, *Phys. Rev. B* **81**, 235113 (2010).
- [40] E. A. Nowadnick, S. Johnston, B. Moritz, R. T. Scalettar, and T. P. Devereaux, *Phys. Rev. Lett.* **109**, 246404 (2012).
- [41] N. C. Costa, K. Seki, S. Yunoki, and S. Sorella, *Commun. Phys.* **3**, 80 (2020).
- [42] S. Barišić, *Phys. Rev. B* **5**, 932 (1972).
- [43] S. Barišić, *Phys. Rev. B* **5**, 941 (1972).
- [44] S. Barišić, J. Labbé, and J. Friedel, *Phys. Rev. Lett.* **25**, 919 (1970).
- [45] S. Li, E. Khatami, and S. Johnston, *Phys. Rev. B* **95**, 121112(R) (2017).
- [46] S. Biermann, L. de' Medici, and A. Georges, *Phys. Rev. Lett.* **95**, 206401 (2005).
- [47] L. de' Medici, S. R. Hassan, M. Capone, and X. Dai, *Phys. Rev. Lett.* **102**, 126401(R) (2009).
- [48] V. Anisimov, I. Nekrasov, D. Kondakov, T. Rice, and M. Sigrist, *Eur. Phys. J. B* **25**, 191 (2002).
- [49] A. Koga, N. Kawakami, T. M. Rice, and M. Sigrist, *Phys. Rev. Lett.* **92**, 216402 (2004).
- [50] B. Gerlach and H. Löwen, *Rev. Mod. Phys.* **63**, 63 (1991).
- [51] V. M. Stojanović and M. Vanević, *Phys. Rev. B* **78**, 214301 (2008).
- [52] D. J. J. Marchand, G. De Filippis, V. Cataudella, M. Berciu, N. Nagaosa, N. V. Prokof'ev, A. S. Mishchenko, and P. C. E. Stamp, *Phys. Rev. Lett.* **105**, 266605 (2010).
- [53] J. Sous, M. Chakraborty, R. V. Krems, and M. Berciu, *Phys. Rev. Lett.* **121**, 247001 (2018).
- [54] E. I. Shneyder, S. V. Nikolaev, M. V. Zotova, R. A. Kaldin, and S. G. Ovchinnikov, *Phys. Rev. B* **101**, 235114 (2020).
- [55] I. A. Makarov, E. I. Shneyder, P. A. Kozlov, and S. G. Ovchinnikov, *Phys. Rev. B* **92**, 155143 (2015).
- [56] E. Shneyder, I. Makarov, M. Zotova, and S. Ovchinnikov, *J. Exp. Theor. Phys.* **126**, 683 (2018).
- [57] C. Castellani, C. DiCastro, D. Feinberg, and J. Ranninger, *Phys. Rev. Lett.* **43**, 1957 (1979).
- [58] M. R. Zirnbauer, *J. Math. Phys.* **62**, 021101 (2021).
- [59] S. A. Trugman, *Phys. Rev. B* **37**, 1597 (1988).
- [60] N. B. Aetukuri, A. X. Gray, M. Drouard, M. Cossale, L. Gao, A. H. Reid, R. Kukreja, H. Ohldag, C. A. Jenkins, E. Arenholz *et al.*, *Nat. Phys.* **9**, 661 (2013).
- [61] A. S. Mishchenko, I. S. Tupitsyn, N. Nagaosa, and N. Prokof'ev, *Sci. Rep.* **11**, 9699 (2021).
- [62] E. Y. Sherman and C. Ambrosch-Draxl, *Phys. Rev. B* **62**, 9713 (2000).
- [63] S. Johnston, F. Vernay, B. Moritz, Z.-X. Shen, N. Nagaosa, J. Zaanen, and T. P. Devereaux, *Phys. Rev. B* **82**, 064513 (2010).